Article ID: 1000-7032(2026)03-0377-09

Phase Distribution Management *via* Green Solvent Engineering for Low-threshold Quasi-2D Perovskite Lasers

WEI Guoqiang[1†], ZHAN Zijun[1†], CAI Shuang[1], ZHOU Hongzhi[1], LIU Zhengzheng[2], HU Zhiping[1*], DU Juan[1*]

(1. *School of Physics and Optoelectronic Engineering, Hangzhou Institute for Advanced Study, University of Chinese Academy of Sciences, Hangzhou* 310024, *China*;
2. *State Key Laboratory of Ultra-intense Laser Science and Technology, Shanghai Institute of Optics and Fine Mechanics, Chinese Academy of Sciences, Shanghai* 201800, *China*)

* *Corresponding Authors, E-mail: huzhiping@ucas. ac. cn; du@ucas. ac. cn*

Abstract: Quasi-two-dimensional (quasi-2d) perovskites are promising gain media for micro-nano lasers, yet their uncontrolled crystallization and abundant low-*n* phases often hinder optical gain and device performance. In this work, we introduce ethyl acetate (EA) as a green antisolvent to fabricate high-quality quasi-2D $PEA_{0.4}MAPbBr_3$ films. The EA-treated films exhibit superior morphology, enhanced crystallinity, and notably inhibited low *n*-phases. These improvements yield a prolonged photoluminescence lifetime of 26. 3 ns and a substantially extended gain lifetime of 129 ps. Consequently, the optimized film exhibits a markedly reduced amplified spontaneous emission (ASE) threshold of 5. 6 $\mu J \cdot cm^{-2}$ and a high net modal gain of 935 cm^{-1}. Leveraging these enhanced gain properties, we successfully demonstrate a vertical-cavity surface-emitting laser (VCSEL) based on a dielectric Bragg reflector microcavity, which delivers single-mode lasing at 528. 3 nm and a high quality factor of ~5 886. This work presents a green-solvent-engineering strategy for high-performance perovskite lasers, advancing their prospects for scalable photonic integration.

Keywords: quasi-2D perovskite; green antisolvent; gain properties; perovskite lasers

CLC number: TN248. 4 **Document code**: A

DOI: 10. 37188/CJL. 20250269 **CSTR**: 32170. 14. CJL. 20250269

绿色溶剂工程调控相分布实现低阈值准二维钙钛矿激光器

魏国强[1†], 占子俊[1†], 蔡 爽[1], 周鸿志[1], 刘征征[2], 胡智萍[1*], 杜 鹃[1*]

(1. 国科大杭州高等研究院 物理与光电工程学院, 浙江 杭州 310024;
2. 中国科学院上海光学精密机械研究所 超强激光科学与技术全国重点实验室, 上海 201800)

摘要: 准二维钙钛矿是微纳激光器的理想增益介质,但其不可控的结晶过程与大量的低 *n* 值相阻碍了其光学增益与器件性能的提升。本研究采用乙酸乙酯(EA)作为一种绿色反溶剂,成功制备了高质量的准二维 $PEA_{0.4}MAPbBr_3$ 薄膜。经 EA 处理后的薄膜表现出更优的形貌、更高的结晶度,并且低 *n* 值相得到了显著抑制。

收稿日期: 2025-12-05; **修订日期**: 2025-12-18

基金项目: 国家自然科学基金(62425502,62375060,62205081,62405073,52272013); 浙江省“领雁”研发攻关计划(2024C01192); 浙江省自然科学基金(LMS25F050001)

Supported by National Natural Science Foundation of China (62425502, 62375060, 62205081, 62405073, 52272013); the “Pioneer” and “Leading Goose” R&D Program of Zhejiang (2024C01192); Zhejiang Provincial Natural Science Foundation (LMS25F050001)

†: 共同贡献作者

这些特性促使钙钛矿薄膜的光致发光寿命延长至26.3 ns,增益寿命显著增加至129 ps。因此,优化后的钙钛矿薄膜表现出显著降低的放大自发辐射(ASE)阈值(5.6 μJ·cm^{-2}),并具有高达935 cm^{-1}的净模态增益。得益于这些增强的增益特性,我们成功制备了基于介质布拉格反射镜微腔的垂直腔面发射激光器,实现了528.3 nm波长的单模激光发射,品质因子高达~5 886。本工作为制备高性能钙钛矿激光器提供了一条绿色溶剂工程策略,并推动了其在光子器件应用中的发展前景。

关 键 词:准二维钙钛矿;绿色反溶剂;增益特性;钙钛矿激光

1 Introduction

Metal halide perovskites have emerged as a promising class of semiconductors for laser applications, owing to their exceptional optoelectronic properties including high optical gain, long carrier lifetimes, and broadly tunable emission wavelengths[1-8]. Among them, quasi-two-dimensional (quasi-2D) perovskites have exhibited outstanding light-emitting performance[9-11], due to their high defect tolerance, high photoluminescence quantum yield (PLQY) and high optical gain coefficient[9-17]. Besides, the natural quantum-well structure of quasi-2D perovskites facilitates rapid and efficient energy funneling from low-*n* to high-*n* domains, promoting the establishment of population inversion[18-21]. These characteristics render quasi-2D perovskites highly promising as laser gain media, enabling low-threshold, room-temperature, and wavelength-tunable micro/nano lasers[5-7]. However, a major challenge remains the typically uncontrolled crystallization process, which often leads to an undesirable abundance of the low-*n* phases[22]. These low-*n* phases act as energy traps, disrupting interphase energy transfer and accelerating material degradation, thereby undermining device stability[23-28]. Additionally, they degrade emission performance by significantly enhancing Auger recombination rates[11], thereby impeding the establishment of population inversion. Therefore, low defect density and well-controlled phase distribution are critical for quasi-2D perovskite film achieving low-threshold and scalable perovskite lasers.

Solvent-engineering is presently one of the most prevalent strategies for producing high-quality perovskite thin films[29-31]. In previous studies, non-coordinating antisolvents such as chlorobenzene (CB) and toluene have been used to accelerate host solvent extraction, modulate nucleation, and steer the crystallization pathway toward dense, uniform grains[32-33]. However, the high toxicity and volatility of these halogenated aromatics raise safety concerns and infrastructure costs for large-scale manufacturing, thereby hindering the commercial adoption of perovskite optoelectronics. Consequently, the development of green antisolvents has been recognized as a key prerequisite for environmentally sustainable perovskite technology[34-35]. Ethyl acetate (EA) has emerged as a particularly attractive candidate owing to its low toxicity, moderate saturated-vapor pressure, and appropriate extraction strength; perovskite light-emitting diodes and solar cells processed with EA already exhibit competitive performance metrics[36-40]. Nonetheless, the influence of EA on the fundamental optical gain properties, phase distribution dynamics, and ultimately the lasing performance of quasi-2D perovskite films remains largely unexplored and poorly understood.

In this work, we employed solvent engineering using EA as a green antisolvent to fabricate high-quality quasi-2D $PEA_{0.4}MAPbBr_3$ films for high-performance vertical-cavity surface-emitting lasers (VCSELs). The EA treatment significantly improved film quality, as evidenced by enlarged grain sizes and enhanced photoluminescence. More importantly, it substantially suppressed low-*n* phases, leading to an accelerated inter-phase energy funneling and a prolonged gain lifetime of 129 ps, as confirmed by transient absorption spectroscopy. These improvements resulted in a notable reduction of the amplified spontaneous emission (ASE) threshold from 11 μJ·cm^{-2} to 5.6 μJ·cm^{-2} and a doubling of the net modal gain from 436 cm^{-1} to 935 cm^{-1}. Capitalizing

on these enhanced gain properties, we successfully constructed a distributed Bragg reflector (DBR)/perovskite/DBR vertical cavity, achieving single-mode lasing with a relatively low threshold of 97.5 $\mu J \cdot cm^{-2}$ and a high-quality factor of ~5 886. This work not only demonstrates a low-threshold VCSEL but also establishes a green-solvent strategy that paves the way for the scalable and sustainable fabrication of perovskite photonic devices.

2 Experiment

2.1 Fabrication of Perovskite Films

Phenylethylammonium bromide (>98%), methylammonium bromide (99.9%) were purchased from Greatcell Solar. Lead(Ⅱ) bromide ($PbBr_2$, 99.999%), ethyl acetate (99.8%), chlorobenzene (99.8%) were purchased from Sigma-Aldrich. All chemicals were directly used without any further purification.

Quartz substrates were sequentially sonicated (30 min each) in de-ionized water, ethanol, acetone and isopropanol, followed by N_2 blow-drying. Immediately before deposition the substrates were oxygen-plasma treated for 5 min (Harrick Plasma PDC-002) to improve perovskite adhesion. All solution preparation and film processing were carried out in a N_2-filled glovebox. For the $PEA_{0.4}MAPbBr_3$: EA film, 0.16 mol/L PEABr, 0.40 mol/L MABr and 0.40 mol/L $PbBr_2$ were dissolved in 1 mL anhydrous DMSO and stirred overnight to afford a clear precursor solution. The solution was passed through a 0.22 μm PTFE syringe filter, and 100 μL were spin-coated onto the pre-cleaned quartz at 4 000 $r \cdot min^{-1}$ for 60 s. During the final 30 s, 100 μL of EA were rapidly dispensed as the antisolvent. The wet film was then annealed at 100 ℃ for 15 min. $PEA_{0.4}MAPbBr_3$: CB films were prepared identically, replacing EA with an equal volume of CB.

2.2 Characterizations

XRD patterns were collected by a Bruker D8 Advance diffractometer with Cu Kα radiation (λ= 0.154 nm). SEM images were collected by ZEISS Gemini SEM 300. AFM images were collected by Bruker Dimension Icon. The absorption spectra of perovskite films were measured by a double-beam UV-Vis spectrophotometer (Model: UV1901PCS, Yoke, China). The steady-state fluorescence spectra of the films were measured by coupling a 405 nm continuous laser into a confocal microscopy system (WITec Alfa 300R) and collecting the fluorescence signals by a WITec ultra-high throughput (UHTS) spectrometer. The fluorescence lifetime was characterized by a home-built micro-spectroscopy system with a 405 nm picosecond pulsed laser (repetition rate tunable). The photoluminescence signals, after excitation light filtration, were coupled to a single-photon counter (TCSPC, PICOQUANT). Time-resolved photoluminescence can be used to obtain the fluorescence lifetime information of perovskite films. The transient absorption spectra were measured by the Helios Fire Ultrafast Systems. For the ASE measurements, the 400 nm excitation pulse is generated by frequency doubling the Ti∶sapphire laser system (35 fs, 1 kHz, 800 nm) through a BBO crystal, the pump beam was shaped into a line spot by a cylindrical lens, then focused onto the sample surface through a slit. The line spot width was adjusted to an appropriate size. The signals emitted by the sample were collected by a lens, passed through a filter to remove pump light, and then focused into a fiber optic spectrometer (USB 4000, Ocean Optics). To obtain slit length-dependent spectra, the slit was closed and then gradually opened to record radiation signals. The net modal gain coefficients were derived by fitting the intensity variation with slit length. Pump fluence-dependent laser emission spectra were recorded under 400 nm femtosecond excitation by the confocal microscopy system.

3 Results and Discussion

Quasi-2D $PEA_{0.4}MAPbBr_3$ films were fabricated *via* spin-coating with the introduction of an anti-solvent. To elucidate the impact of the anti-solvent on film formation, we systematically compared the properties of films processed with CB and EA. Scanning electron microscopy (SEM) images (Fig. 1(a) and 1(b)) reveal that the EA-treated film possesses a markedly smoother and denser morphology compared to

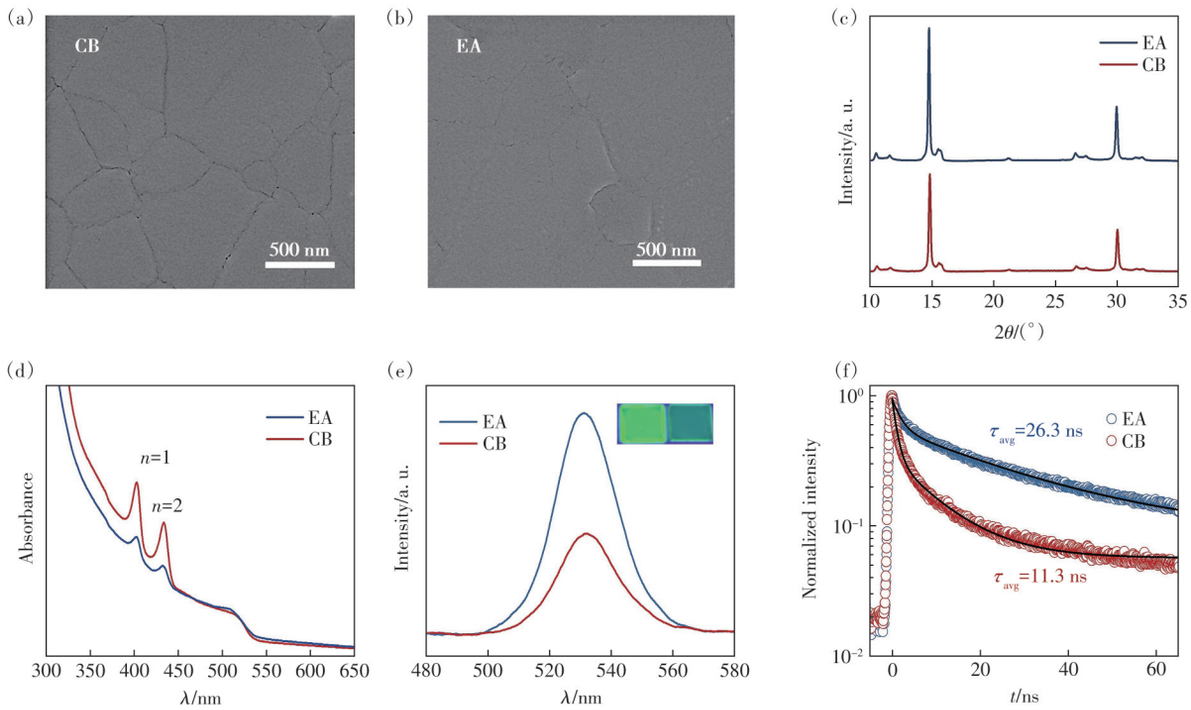

Fig.1 (a)-(b)SEM images of CB- and EA-treated films. (c)XRD patterns, (d)UV-visible absorption spectra, (e)PL spectra, and (f)TRPL decay curves of CB- and EA-treated films

its CB-treated counterpart. AFM measurements show that the roughness of the EA-treated film and the CB-treated film is 7.46 nm and 4.95 nm (Fig. S3), respectively. The corresponding XRD (X-ray diffraction) patterns in Fig. 1(c) show that the EA-treated film exhibits more intense and sharper diffraction peaks with a narrower full width at half-maximum (FWHM), indicating superior crystallinity. The absorption spectra (Fig. 1(d)) display characteristic peaks around 403 nm and 434 nm, corresponding to the n=1 and n=2 excitonic phases of the quasi-2D perovskite, respectively. Notably, the intensities of low n-phase (n=1 and n=2) peaks are suppressed in the EA-treated film, suggesting a more favorable phase distribution. Consequently, the EA-treated film exhibits a significant boost in photoluminescence (PL) intensity (Fig. 1(e)). Time-resolved PL (TRPL) measurements (Fig. 1(f)) reveal an average carrier lifetime of 26.3 ns for the EA-treated film, substantially longer than the 11.3 ns observed for the EA-treated film (fitting parameters in Tab. S1). This prolonged lifetime unequivocally demonstrates the effective suppression of non-radiative recombination channels in the EA-treated film.

Benefitting from the significantly improved film quality and precisely controlled crystalline phase of the quasi-2D perovskite, the EA-treated perovskite exhibits markedly enhanced ASE performance. To systematically evaluate the optical gain properties, we performed femtosecond laser pumping at 400 nm on both $PEA_{0.4}MAPbBr_3$:CB and $PEA_{0.4}MAPbBr_3$:EA films. As shown in Fig. 2(a), the evolution of the emission spectra of the $PEA_{0.4}MAPbBr_3$:CB film under increasing pump fluence reveals a clear transition from broad spontaneous emission to narrowband ASE. At low excitation densities, the film exhibits a spontaneous emission peak centered at ~530.2 nm, with a full width at half maximum (FWHM) of about 27 nm. As the pump intensity rises, a sharp ASE peak emerges at 540.7 nm, accompanied by a notable spectral narrowing, with the FWHM reduced to ~4.5 nm. The corresponding plot of output intensity and FWHM as a function of pump fluence (Fig. 2(b)) suggest an ASE threshold of 11 μJ·cm^{-2}. In contrast, the EA-treated $PEA_{0.4}MAPbBr_3$:EA film displays a similar trend of spectral evolution from spontaneous emission to ASE (Fig. 2(d)), with the ASE peak positioned ~543.4 nm and a FWHM

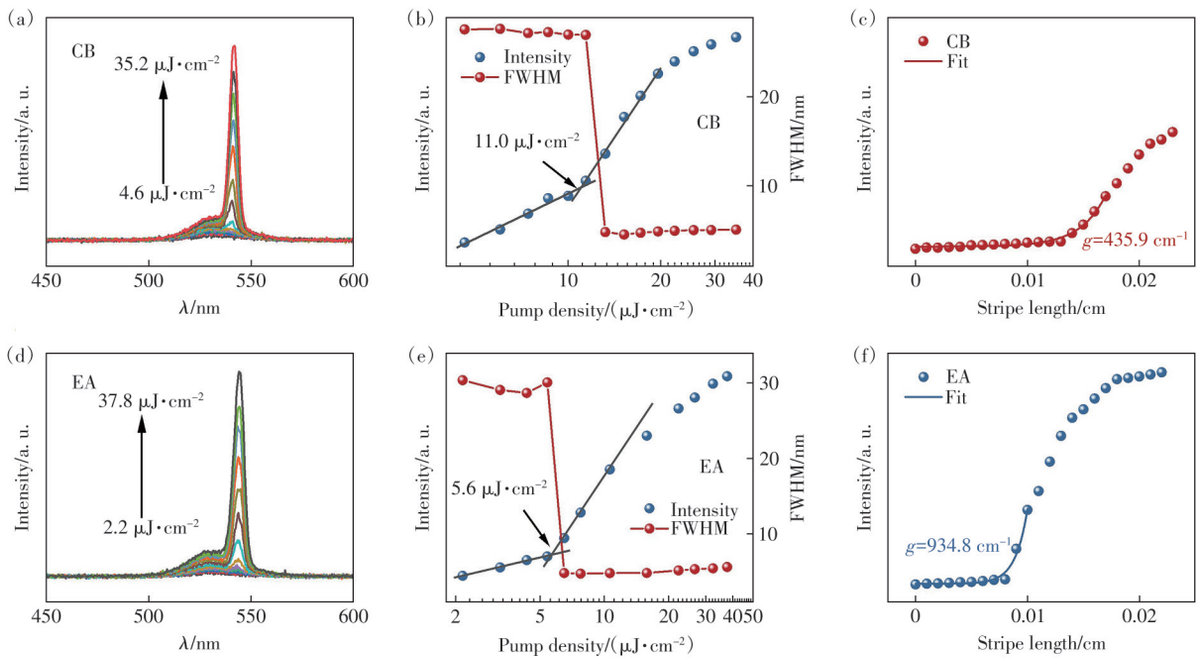

Fig.2　Stimulated-emission characteristics of $PEA_{0.4}MAPbBr_3$ films processed with different antisolvents. (a), (d) Pump-fluence-dependent emission spectra for (a) CB- and (d) EA-treated films. (b), (e) Integrated emission intensity (left axis) and full width at half maximum (FWHM; right axis) as functions of pump fluence for the CB- and EA-treated films, respectively. (c), (f) Edge-emission intensity *versus* stripe length obtained from variable-stripe-length measurements for the CB- and EA-treated films, respectively

of ~4. 8 nm. Remarkably, as summarized in Fig. 2(e), the ASE threshold of the $PEA_{0.4}MAPbBr_3$: EA film is significantly reduced to 5. 6 μJ·cm^{-2}, underscoring the beneficial role of EA treatment in enhancing optical gain while reducing lasing requirements.

The optical gain coefficient is a crucial factor determining the performance of the laser gain medium. To quantitatively compare the intrinsic gain properties, we employed the variable stripe length (VSL) method to obtain stripe-length-dependent emission spectra of perovskite films (Fig. S1). As depicted in Fig. 2(c) and 2(f), the $PEA_{0.4}MAPbBr_3$: CB film exhibits a gain coefficient of 435. 9 cm^{-1} at a pump fluence of 10 times its ASE threshold ($10P_{th}$). In contrast, the gain coefficient of $PEA_{0.4}MAPbBr_3$: EA is 934. 8 cm^{-1} at $10P_{th}$, which is 2. 26 times greater than that of its CB-treated counterpart. The increased gain coefficient of $PEA_{0.4}MAPbBr_3$: EA confirms that the EA anti-solvent engineering effectively enhances the optical gain by mitigating loss pathways and improving the perovskite film intrinsic quality.

To reveal the mechanisms of the enhanced optical amplification properties of quasi-2D perovskite films, ultrafast transient absorption (TA) spectroscopy measurements are performed, as shown in Fig. 3. Both CB- and EA-treated $PEA_{0.4}MAPbBr_3$ films (Fig. 3(a) and 3(b)) exhibit four distinct ground-state bleaching (GSB) signals at 403, 434, 464, 518 nm. These correspond to the n=1, 2, 3, $n\geqslant4$ phases, respectively, indicating state filling from photoexcited excitons in these different n-value phases. The evolution of the spectral features at different delay time is extracted in Fig. 3(c) and 3(d), the GSB signals for n=2 and $\geqslant4$ are the dominant components. To illustrate the differences in phase distribution between the two perovskite films, Fig. S2 depicts their TA spectra at 0. 5 ps, revealing a significant difference in the signal intensity of the low-dimensional phase (n=2) between the CB- and EA-treated perovskite films. The ratio of the GSB signals from the n=2 to the $n\geqslant4$ phase was 1. 44 for the CB-treated film and 0. 92 for the EA-treated film, indicating that the n=2 phase is suppressed by the EA treatment. Fig. 3(e) and 3(f) describe the

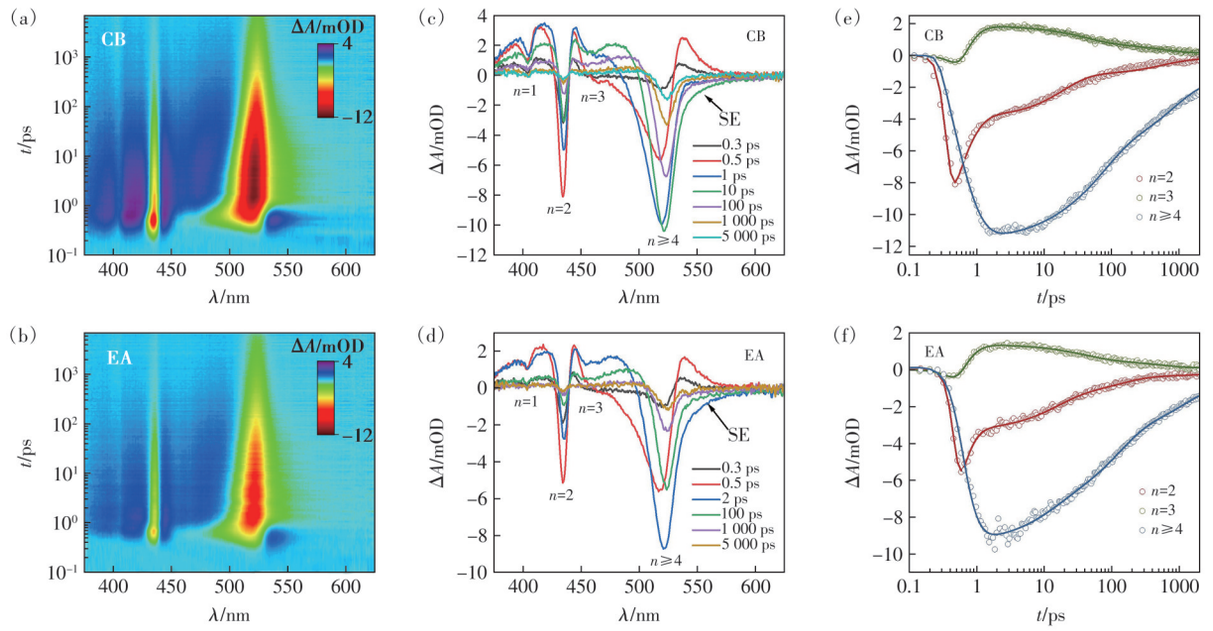

Fig.3 TA spectra of the CB- and EA-treated perovskite films. 2D pseudo-color TA images of (a)CB- and (b)EA-treated perovskite film. TA spectra of the (c)CB- and (d)EA-treated perovskite film at different time delays. TA kinetics probe of (e)CB- and (f)EA-treated perovskite film at different wavelengths

representative GSB kinetics corresponding to different *n*-phase components. The fitting results reveal fast-decay lifetime of 0.266 ps (*n*=2) and 0.299 ps (*n*=3) for the EA-treated films, faster than the corresponding values of 0.367 ps (*n*=2) and 0.487 ps (*n*=3) measured for the CB-treated films. Simultaneously, the rise time of the *n*≥4 phase decreases from 0.394 ps (CB) to 0.279 ps (EA), representing an acceleration of nearly 30%. These results indicate a more efficient carrier transfer process in the EA-treated perovskite films, promoting exciton accumulation in the *n*>4 phase, which is beneficial for reducing the thresholds of ASE and lasers[19,23]. As depicted in Fig. 3(c) and 3(d), a rapid transition of the photoinduced absorption (PIA) signal from positive to negative was observed in the range of 530 nm to 550 nm, indicating the establishment of the stimulated emission arising from population inversion. To further analyze the temporal dynamics of optical gain in both films, the TA kinetics probed at the ASE wavelength of both perovskite films are plotted in Fig. S2. The gain lifetime of the EA-treated film reaches 129 ps, which is much longer than that of CB-treated one (86 ps). The extended gain lifetime facilitates the establishment of population inversion, resulting an enhanced optical gain property of EA-treated perovskite films.

Leveraging the superior gain of the EA-treated film, we realized a single-mode VCSEL by embedding a $PEA_{0.4}MAPbBr_3$ layer between two dielectric Bragg reflectors (DBR/perovskite/DBR; Fig. 4(a), the reflection curve of the DBR is shown in Fig. S4. Pump fluence dependent spectra were recorded under 400 nm, 1 kHz femtosecond excitation (Fig. 4(b)) show only broad spontaneous emission (FWHM≈1.2 nm) below threshold. As the fluence exceeds the critical value, a razor-sharp line (FWHM≈0.09 nm) appears and the peak shifts to 528.3 nm (Fig. 4(d)), with a quality factor of 5 886. The nonlinear rise in output intensity and the concurrent linewidth collapse (Fig. 4(c)) suggest the laser threshold of 97.5 $\mu J \cdot cm^{-2}$. The laser polarization degree is 85.2% (Fig. S5). Lasing from $PEA_{0.4}MAPbBr_3$ has scarcely been reported. Our device exhibits comparatively favorable performance, compared to analogous $MAPbBr_3$ film-based lasers, highlighting the efficacy of the EA antisolvent strategy.

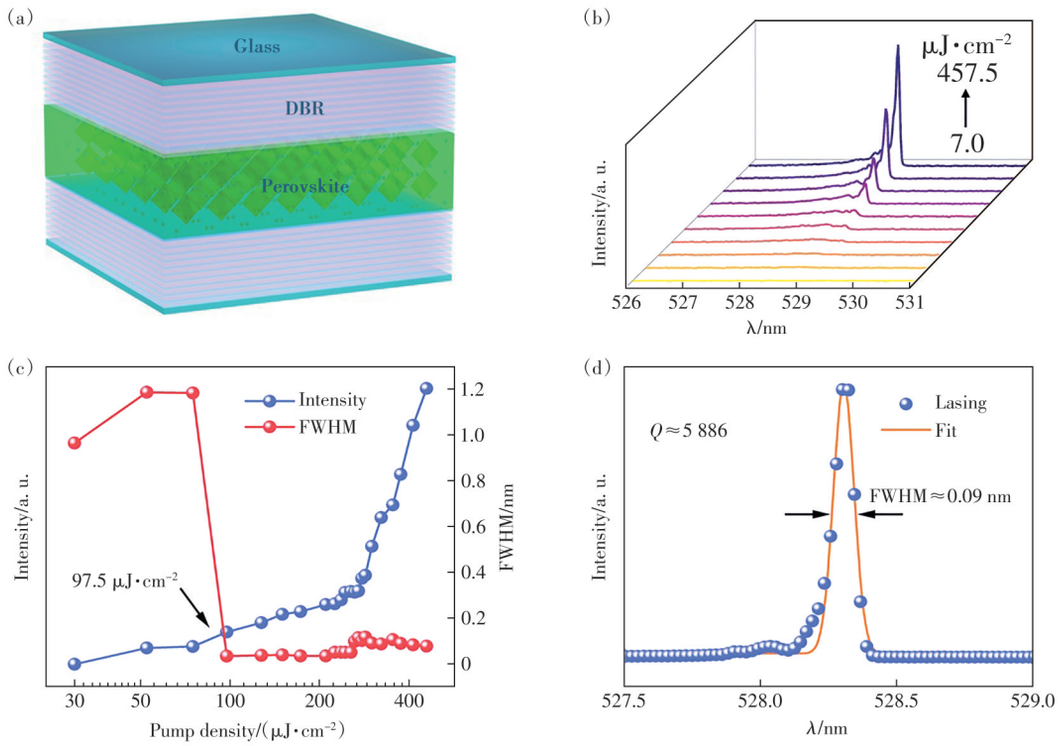

Fig.4　(a) Schematic layout of VCSEL device. (b) Emission spectra *versus* pump fluence under 400 nm femtosecond excitation. (c) Pump-fluence dependence of output intensity (left axis) and full width at half maximum (right axis). (d) Lasing spectrum and Gaussian fit of the lasing

4　Conclusion

In summary, we demonstrate that the EA antisolvent treatment effectively suppresses the formation of low *n*-phases, improves crystallinity, and enhances photoluminescence. TA spectroscopy reveals that EA treatment can accelerate carrier funneling into high-*n* wells and extends the gain lifetime from 86 ps to 129 ps. These favorable changes collectively reduce the ASE threshold by 49% (from 11 μJ·cm^{-2} to 5.6 μJ·cm^{-2}), double the optical gain lifetime, and elevate the net modal gain from 436 cm^{-1} to 935 cm^{-1}. Benefitting from these enhancements, we successfully realized a VCSEL based on a dielectric Bragg reflector microcavity, which achieves single-mode lasing with a high-quality factor of ~5 886. Our findings elucidate the origin of the gain enhancement enabled by EA and establish green-antisolvent processing as a viable and sustainable strategy for realizing low-threshold perovskite lasers.

Supplementary Information and Response Letter are available for this paper at: http://cjl.lightpublishing.cn/thesisDetails#10.37188/CJL.20250269

References:

[1] ZHANG S T, YI C, WANG N N, *et al.* Efficient red perovskite light-emitting diodes based on solution-processed multiple quantum wells [J]. *Adv. Mater.*, 2017, 29(22): 1606600.

[2] TRAORE B, PEDESSEAU L, ASSAM L, *et al.* Composite nature of layered hybrid perovskites: assessment on quantum and dielectric confinements and band alignment [J]. *ACS Nano*, 2018, 12(4): 3321-3332.

[3] ZHANG L, SUN C J, HE T W, *et al.* High-performance quasi-2D perovskite light-emitting diodes: from materials to devices [J]. *Light: Sci. Appl.*, 2021, 10(1): 61.

[4] QUAN L N, YUAN M J, COMIN R, *et al.* Ligand-stabilized reduced-dimensionality perovskites [J]. *J. Am. Chem. Soc.*, 2016, 138(8): 2649-2655.

[5] ZHANG D Z, FU Y X, ZHAN H M, *et al*. Suppressing thermal quenching *via* defect passivation for efficient quasi-2D perovskite light-emitting diodes [J]. *Light*: *Sci. Appl.*, 2022, 11(1): 69.

[6] JIN G R, LIU T H, LI Y Z, *et al*. Low-dimensional phase suppression and defect passivation of quasi-2D perovskites for efficient electroluminescence and low-threshold amplified spontaneous emission [J]. *Nanoscale*, 2022, 14(3): 919-929.

[7] GUO Z Y, ZHANG Y, WANG B Z, *et al*. Promoting energy transfer *via* manipulation of crystallization kinetics of quasi-2D perovskites for efficient green light-emitting diodes [J]. *Adv. Mater.*, 2021, 33(40): 2102246.

[8] CHU Z M, YE Q F, ZHAO Y, *et al*. Perovskite light-emitting diodes with external quantum efficiency exceeding 22% *via* small-molecule passivation [J]. *Adv. Mater.*, 2021, 33(18): 2007169.

[9] HU Z P, LIU Z Z, ZHAN Z J, *et al*. Advances in metal halide perovskite lasers: synthetic strategies, morphology control, and lasing emission [J]. *Adv. Photon.*, 2021, 3(3): 034002.

[10] LIN K B, XING J, QUAN L N, *et al*. Perovskite light-emitting diodes with external quantum efficiency exceeding 20 per cent [J]. *Nature*, 2018, 562(7726): 245-248.

[11] JIANG Y Z, CUI M H, LI S S, *et al*. Reducing the impact of Aauger recombination in quasi-2D perovskite light-emitting diodes [J]. *Nat. Commun.*, 2021, 12(1): 336.

[12] 汪俊, 周奉献, 李骞, 等. 准二维铅基钙钛矿微纳激光器 [J]. 发光学报, 2022, 43(11): 1645-1662.
WANG J, ZHOU F X, LI Q, *et al*. Quasi-2D lead halide perovskites for micro- and nanolasers [J]. *Chin. J. Lumin.*, 2022, 43(11): 1645-1662. (in English)

[13] LIU Z Z, HU M C, DU J, *et al*. Subwavelength-polarized quasi-two-dimensional perovskite single-mode nanolaser [J]. *ACS Nano*, 2021, 15(4): 6900-6908.

[14] ZHANG Q, DIEDERICHS C, XIONG Q H. Golden hour for perovskite photonics [J]. *Photonics Res.*, 2020, 8(12): 1-4.

[15] LI X H, LIU W W, SONG Y L, *et al*. Two-photon-pumped high-quality, single-mode vertical cavity lasing based on perovskite monocrystalline films [J]. *Nano Energy*, 2020, 68: 104334.

[16] LI M L, SHANG Q Y, LI C, *et al*. High optical gain of solution-processed mixed-cation $CsPbBr_3$ thin films towards enhanced amplified spontaneous emission [J]. *Adv. Funct. Mater.*, 2021, 31(25): 2102210.

[17] XING G C, MATHEWS N, LIM S S, *et al*. Low-temperature solution-processed wavelength-tunable perovskites for lasing [J]. *Nat. Mater.*, 2014, 13(5): 476-480.

[18] YUAN M J, QUAN L N, COMIN R, *et al*. Perovskite energy funnels for efficient light-emitting diodes [J]. *Nat. Nanotechnol.*, 2016, 11(10): 872-877.

[19] JIANG Y Z, WEI J L, YUAN M J. Energy-funneling process in quasi-2D perovskite light-emitting diodes [J]. *J. Phys. Chem. Lett.*, 2021, 12(10): 2593-2606.

[20] LI M L, GAO Q G, LIU P, *et al*. Amplified spontaneous emission based on 2D ruddlesden-popper perovskites [J]. *Adv. Funct. Mater.*, 2018, 28(17): 1707006.

[21] LEI L, SEYITLIYEV D, STUARD S, *et al*. Efficient energy funneling in quasi-2D perovskites: from light emission to lasing [J]. *Adv. Mater.*, 2020, 32(16): 1906571.

[22] DING S, WANG Q Q, GU W C, *et al*. Phase dimensions resolving of efficient and stable perovskite light-emitting diodes at high brightness [J]. *Nat. Photonics*, 2024, 18(4): 363-370.

[23] 叶子青, 张灯亮, 段兴兴, 等. 基于氟代苯乙胺有机阳离子的准二维钙钛矿发光二极管 [J]. 发光学报, 2022, 43(8): 1244-1255.
YE Z Q, ZHANG D L, DUAN X X, *et al*. Quasi-2D perovskite light-emitting diodes with fluorophenethylammonium as organic cations [J]. *Chin. J. Lumin.*, 2022, 43(8): 1244-1255. (in Chinese)

[24] HUANG S H, LIU N, LIU Z Z, *et al*. Enhanced amplified spontaneous emission in quasi-2D perovskite by facilitating energy transfer [J]. *ACS Appl. Mater. Interfaces*, 2022, 14(29): 33842-33849.

[25] WU C, WU T, YANG Y G, *et al*. Alternative type two-dimensional-three-dimensional lead halide perovskite with inorganic sodium ions as a spacer for high-performance light-emitting diodes [J]. *ACS Nano*, 2019, 13(2): 1645-1654.

[26] GUO Y W, JIA Y H, LI N, *et al*. Degradation mechanism of perovskite light-emitting diodes: an *in situ* investigation *via* electroabsorption spectroscopy and device modelling [J]. *Adv. Funct. Mater.*, 2020, 30(19): 1910464.

[27] LIANG Y, SHANG Q Y, WEI Q, *et al*. Lasing from mechanically exfoliated 2D homologous Ruddlesden-Popper

perovskite engineered by inorganic layer thickness [J]. *Adv. Mater.*, 2019, 31(39): 1903030.

[28] 陈月花, 向勋勋, 蒋劲舟, 等. 准二维钙钛矿相分布调控及其蓝光发光二极管 [J]. 发光学报, 2025, 46(12): 2325-2333.
CHEN Y H, XIANG X X, JIANG J Z, *et al.* Regulating phase distribution of quasi-two-dimensional perovskites for blue light-emitting diodes [J]. *Chin. J. Lumin.*, 2025, 46(12): 2325-2333. (in Chinese)

[29] JEON N J, NOH J H, KIM Y C, *et al.* Solvent engineering for high-performance inorganic-organic hybrid perovskite solar cells [J]. *Nat. Mater.*, 2014, 13(9): 897-903.

[30] LIANG Y, SHANG Q Y, LI M L, *et al.* Solvent recrystallization-enabled green amplified spontaneous emissions with an ultra-low threshold from pinhole-free perovskite films [J]. *Adv. Funct. Mater.*, 2021, 31(48): 2106108.

[31] 董威, 李静, 尹文旭, 等. 准二维钙钛矿生长控制:结构依赖的激子与电荷行为 [J]. 发光学报, 2024, 45(11): 1767-1781.
DONG W, LI J, YIN W X, *et al.* Growth control of quasi-two-dimensional perovskites: structure-dependent exciton and charge behavior [J]. *Chin. J. Lumin.*, 2024, 45(11): 1767-1781. (in English)

[32] AHN N, SON D Y, JANG I H, *et al.* Highly reproducible perovskite solar cells with average efficiency of 18.3% and best efficiency of 19.7% fabricated *via* lewis base adduct of lead(Ⅱ) iodide [J]. *J. Am. Chem. Soc.*, 2015, 137(27): 8696-8699.

[33] ZHOU Y Y, YANG M J, WU W W, *et al.* Room-temperature crystallization of hybrid-perovskite thin films *via* solvent-solvent extraction for high-performance solar cells [J]. *J. Mater. Chem.* A, 2015, 3(15): 8178-8184.

[34] ZHANG W Y, LI Y C, LIU X, *et al.* Ethyl acetate green antisolvent process for high performance planar low-temperature SnO_2-based perovskite solar cells made in ambient air [J]. *Chem. Eng.* J., 2020, 379: 122298.

[35] CUI Y Y, WANG S R, DING L M, *et al.* Green-solvent-processable perovskite solar cells [J]. *Adv. Energy Sustain. Res.*, 2021, 2(2): 2000047.

[36] ZHANG X P, LI X Y, TAO L, *et al.* Precise control of crystallization and phase-transition with green anti-solvent in wide-bandgap perovskite solar cells with open-circuit voltage exceeding 1.25 V [J]. *Small*, 2023, 19(22): e2208289.

[37] XU Y S, WANG H L, CHEN Y, *et al.* Efficient sky-blue light-emitting diodes based on oriented perovskite nanoplates [J]. *Adv. Opt. Mater.*, 2022, 10(1): 2101525.

[38] XU L B, CHE S Y, HUANG J Y, *et al.* Towards green antisolvent for efficient $CH_3NH_3PbBr_3$ perovskite light emitting diodes: a comparison of toluene, chlorobenzene, and ethyl acetate [J]. *Appl. Phys. Lett.*, 2019, 115(3): 033101.

[39] LI J H, HUA X D, GAO F, *et al.* Green antisolvent additive engineering to improve the performance of perovskite solar cells [J]. *J. Energy Chem.*, 2022, 66: 1-8.

[40] KIM S, JEONG I, PARK C, *et al.* Morphology control of perovskite in green antisolvent system for $MAPbI_3$-based solar cells with over 20% efficiency [J]. *Sol. Energy Mater. Sol. Cells*, 2019, 203: 110197.

魏国强(2001–),男,四川宜宾人,硕士研究生,2023年于常州大学获得学士学位,主要从事卤化物钙钛矿LED及激光器件的研究。
E-mail: weiguoqiang23@mails.ucas.ac.cn

胡智萍(1991–),女,河南新乡人,博士,副研究员,硕士生导师,2018年于重庆大学获得博士学位,主要从事新型光电材料与器件、激光材料与微纳激光器的研究。
E-mail: huzhiping@ucas.ac.cn

占子俊(1990–),男,湖北黄冈人,博士,2024年于同济大学获得博士学位,主要从事新型卤化物半导体激光材料与发光器件的研究。
E-mail: zhanzijun@ucas.ac.cn

杜鹃(1980–),女,山东潍坊人,博士,研究员,博士生导师,2007年于中国科学院上海光学精密机械研究所获得博士学位,主要从事超短脉冲激光与功能材料相互作用(包括新型发光材料与器件、微纳激光与光电子器件、太阳能电池材料与器件及材料内超快动力学)的研究。
E-mail: du@ucas.ac.cn